Improving three-dimensional target reconstruction in the multiple scattering regime using the decomposition of the time-reversal operator

Ting Zhang, Patrick C. Chaumet, Anne Sentenac, and Kamal Belkebir

Citation: J. Appl. Phys. **120**, 243101 (2016); doi: 10.1063/1.4972470
View online: http://dx.doi.org/10.1063/1.4972470
View Table of Contents: http://aip.scitation.org/toc/jap/120/24
Published by the American Institute of Physics

Improving three-dimensional target reconstruction in the multiple scattering regime using the decomposition of the time-reversal operator

Ting Zhang,[1,2] Patrick C. Chaumet,[1] Anne Sentenac,[1] and Kamal Belkebir[1]
[1]*Aix Marseille Université, CNRS, Centrale Marseille, Institut Fresnel, UMR 7249, 13013 Marseille, France*
[2]*Sorbonne Universités, UPMC Univ Paris 06, UR2, L2E, F-75005 Paris, France*

(Received 7 September 2016; accepted 5 December 2016; published online 22 December 2016)

The singular vectors of the time reversal operator (décomposition de l'opérateur de retournement temporel, time reversal operator decomposition (DORT) processing) are often used for localizing small echogeneous targets in a cluttered environment. In this work, we show that they can also improve the imaging of relatively large and contrasted targets in a homogeneous environment. It is observed that non-linear inversion schemes, minimizing iteratively the discrepancy between experimental data and simulated field scattered by target estimates, are more efficient when the illuminations correspond to the DORT singular vectors. In addition, DORT preprocessing permits a drastic diminution of the data load and computer burden. This study is conducted with experimental microwave data of targets with size comparable or greater than the wavelength. *Published by AIP Publishing.*
[http://dx.doi.org/10.1063/1.4972470]

I. INTRODUCTION

In the last two decades, a wealth of research has been devoted to the development of inverse techniques that reconstruct targets from their electromagnetic (either microwave or optical) scattered far-field measured for different illuminations. This task is particularly difficult when the field inside the target differs significantly from the illumination due to multiple scattering. This challenge is particularly interesting as accounting for multiple scattering in the inversion model could ameliorate the image resolution.[1] In this case, the inverse problem becomes non-linear and ill-posed and requires sophisticated reconstruction techniques. The latter generally estimates iteratively the permittivity distribution of the target within a given investigating domain so as to minimize a cost functional representing the distance between the data and the simulated field scattered by the estimate. Two main approaches can be distinguished. The linearized one assumes that, at each iteration step, the field in the investigating domain is the solution of the forward scattering problem for the best available target estimation.[2–4] On the other hand, the non-linearized ones consider the field in the investigation domain as an additional parameter that is estimated together with the permittivity distribution thanks to a minimization procedure.[5,6] A third approach, known as the hybrid method (HM) in Ref. 6, combines both methods for benefiting from the robustness of the non-linearized technique with the rapidity of the linearized one. However, despite these different developments, the accurate inversion of scattering data stemming from relatively large and contrasted targets is not always ensured. To improve the inversion performances, a popular technique relying on *a priori* information on the sample consists in adding regularization terms to the cost functional.[7,8] In this work, we propose a complementary approach based on the optimization of the illuminations through the singular value decomposition (SVD) of the scattering operator.

In most imaging experiments, the sample scattered field is recorded on many observation points for different illuminations. These illuminations may correspond to the field emitted by antennas placed at various positions or to collimated beams coming under various angles. In any case, they do not depend on the sample. Now, using illuminations that focus preferentially on the sample is *a priori* more efficient for collecting useful data on the sample.[9,10] This can be done using the décomposition de l'opérateur de retournement temporel, time reversal operator decomposition technique (DORT), which consists in backpropagating the dominant singular vectors of the scattering operator. DORT has been widely used to detect, localize, and image small (compared to the wavelength) echogeneous targets buried in a cluttered environment.[5,11–15] It has been shown in this case that the number of dominant singular values is directly linked to the number of echogeneous targets and that the associated singular vectors correspond to waves focusing on the targets.

In this work, we consider relatively large and scattering targets in a homogeneous environment. The imaging difficulty does not come from the structural or external noise but from the presence of multiple scattering which requires non-linear or linearized inversion schemes to be handled properly. We show that introducing the DORT technique in the reconstruction schemes ameliorates significantly the target reconstruction and, in addition, decreases the computation time.

In the following, we first describe the DORT approach. Then, we rapidly sketch different inversion schemes accounting for multiple scattering and recall how DORT preprocessing can be introduced in the iterative reconstruction.[5] Lastly, we apply the inversion tools with

and without DORT preprocessing to experimental microwave data.

II. SINGULAR VALUE DECOMPOSITION OF THE SCATTERING OPERATOR

We consider a multistatic imaging experiment operating at a single angular frequency ω. In the experiment, the target is assumed to be confined in a known bounded region Ω. The target is successively illuminated by $l = 1, \ldots, L$ emitters placed at $\mathbf{r}_l$ and polarized along $\hat{\mathbf{e}}_l^{\text{inc}}$. For each illumination, $q = 1, \ldots, Q$ receivers, placed at $\mathbf{r}_q$ and oriented along $\hat{\mathbf{e}}_q$, measure the projection of its scattered field onto $\hat{\mathbf{e}}_q$. Thus, for the l-th illumination, Q scalar data are recorded and gathered in a scattered field vector denoted by $\mathbf{f}_l^{\text{mes}} = [f_{l,1}^{\text{mes}}, \ldots, f_{l,Q}^{\text{mes}}]^t$ where ^{t} denotes the transposed vector. The scattering matrix $\mathbf{K}$ is built such that $\mathbf{K}_{lq}$ represents the scalar projection of the scattered field measured at the q-th receiver for the l-th emitter. The Singular Value Decomposition (SVD) of the $L \times Q$ scattering matrix $\mathbf{K}$ yields a set of singular real values σ_p, $p = 1, \ldots, \min(L, Q)$, associated with singular vectors of dimension Q, $\mathbf{v}_p$ and singular vectors of dimension L, $\mathbf{u}_p$, such that, whatever the vector $\mathbf{x}$ of dimension Q

$$\mathbf{K}\mathbf{x} = \sum_{p=1}^{\min(L,Q)} \mathbf{u}_p \sigma_p [\mathbf{v}_p^t . \mathbf{x}]. \tag{1}$$

A similar expression is obtained for any vector $\mathbf{y}$ of dimension L by interchanging the role of $\mathbf{u}_p$ and $\mathbf{v}_p$ and replacing $\mathbf{K}$ by its transpose. The Q-vector $\mathbf{K}^t\mathbf{y}$ is the scattered field vector that would be measured on the Q receivers if the amplitudes $\mathbf{y}$ were put on the L emitters. Thanks to the reciprocity theorem, the role of the emitters and receivers is interchangeable so that the L-vector $\mathbf{K}\mathbf{x}$ can be considered as the scattered field vector on the L emitters (playing the role of receivers) when the amplitudes $\mathbf{x}$ are put on the Q receivers (playing the role of emitters).[13,16,17]

The analysis of the singular values permits us to distinguish the singular vectors that convey useful information on the target from those that are mostly noise.[18] Hereafter, we call N_{DORT} the number of dominant singular values which separates the signal space from the noise space.

When the targets are small compared to the wavelength, the number of dominant singular values is equal to the number of targets times the polarization of the antennas, and it is relatively easy to distinguish the singular vectors belonging to the signal space from that belonging to the noise space. It has been shown that the backpropagation of these dominant singular vectors generates illuminations that focus on the targets, even when the latter are placed in a cluttered environment.[5,14,19] Keeping only the data corresponding to the dominant singular vectors in an ill-posed inverse problem has also been shown to act as a Tikhonov regularization under certain conditions.[20,21]

When the size of the scatterer is comparable to or larger than the wavelength, the number of dominant singular values is not simply linked to the number of scatterers, and it becomes more difficult to distinguish the signal space from the noise space. In this case, it has been proposed to keep all the singular vectors in the process but to weight their contribution with their singular value.[22] This approach is particularly adapted to our imaging experiment where the targets are relatively large and contrasted. Hereafter, the data processing uses exclusively the singular vectors multiplied by their singular value, which are called DORT vectors. It is worth noting at this point that the weighting of the singular vectors can be combined with a discarding of the "noisy" singular vectors (if the behavior of the singular values permits a clear demarcation between the signal and noise spaces). This is an important feature of our data processing, which will be discussed in the "Reconstruction" section.

The focusing DORT incident field can be either calculated with the Q-vector $\mathbf{v}_p$ or the L-vector $\mathbf{u}_p$. In our experimental configuration where $Q > L$, it is more interesting to use $\mathbf{v}_p$ to generate the DORT illuminations and to detect the scattered field on the L emitters as it decreases the number of data to $N_{\text{DORT}} \times L$ (in place of $N_{\text{DORT}} \times Q$).

For one position vector $\mathbf{r}$ inside the investigating domain Ω, the focusing DORT incident field can be written as

$$\mathbf{E}_p^{\text{DORT}}(\mathbf{r}) = \sum_{q=1}^{Q} \sigma_p v_{p,q} \mathbf{G}(\mathbf{r}, \mathbf{r}_q) \hat{\mathbf{e}}_q, \tag{2}$$

where $\mathbf{G}(\mathbf{r}, \mathbf{r}_q)\mathbf{p}$ represents the field at $\mathbf{r}$ emitted by a dipole $\mathbf{p}$ located at $\mathbf{r}_q$. The corresponding scattered field detected on the L emitters, $\mathbf{f}_p^{\text{DORT}}$ associated with the DORT incident field $\mathbf{E}_p^{\text{DORT}}$, is equal to $\mathbf{K}\mathbf{v}_p$ and reads

$$\mathbf{f}_{p,l}^{\text{DORT}} = \sum_{q=1}^{Q} \sigma_p v_{p,q} f_{l,q}^{\text{mes}} \hat{\mathbf{e}}_q. \tag{3}$$

The DORT preprocessing consists in forming a set of data $\mathbf{f}_p^{\text{DORT}}$ for the N_{DORT} dominant singular values from the measured $\mathbf{f}^{\text{mes}}$.

III. THE INVERSION PROBLEM

The realm of inverse scattering problems is to determine the relative permittivity distribution of samples from the measured scattered field. In this study, we consider the imaging of targets that support multiple scattering. In this case, the reconstruction of the target generally requires the rigorous solving of Maxwell equations for the different permittivity estimates (forward problem). The Maxwell solver is usually at the core of the inversion algorithm.

A. The forward problem

In our approach, the forward problem is solved thanks to the Discrete Dipole Approximation (DDA).[23,24] Since this method is well known, it is only briefly described to settle the notation used for the inverse scattering problem.

The object is described by a permittivity contrast distribution $\chi = \varepsilon - \varepsilon_b$, which is defined as the difference between the object relative permittivity ε and the background medium ε_b. It is assumed that χ is null outside a bounded investigating region Ω. The DDA consists in discretizing

Ω into M small subunits so as to cast the Maxwell equations into a self-consistent linear system, written in operator notation

$$\mathbf{E} = \mathbf{E}^{\text{inc}} + \mathbf{A}\chi\mathbf{E} \tag{4}$$

that is solved numerically. In Eq. (4), χ is a diagonal matrix $\chi_{mm} = \chi(\mathbf{r}_m)$, $\mathbf{A}$ is a square matrix of size $(3M \times 3M)$ of general term $\mathbf{G}(\mathbf{r}_m, \mathbf{r}'_m)$, and $\mathbf{E}$ and $\mathbf{E}^{\text{inc}}$ are the total field and the incident field, respectively. The scattered field corresponding to the l-th illumination can be written in the following condensed form:

$$\mathbf{E}_l^{\text{d}} = \mathbf{B}\chi\mathbf{E}_l, \tag{5}$$

where $l = 1, \ldots, L$, and $\mathbf{B}$ is a matrix of size $(3M \times 3Q)$. The matrix $\mathbf{B}$ contains the Green function $\mathbf{G}^{\text{d}}(\mathbf{r}_q, \mathbf{r}_m)$, where $\mathbf{r}_m$ denotes a point in the scattering domain, $m = 1, \ldots, M$, while $\mathbf{r}_q$ is an observation point, $q = 1, \ldots, Q$. Note that $\mathbf{B}$ does not depend on the angle of incidence.

B. Inversion schemes

The reconstruction of the target permittivity distribution from the measured scattered field in the multiple scattering regime corresponds to a nonlinear and ill-posed inverse problem. The most popular strategies consist to determine the parameters of interest iteratively. In the present paper, two iterative schemes have been applied. The first one is a classical linearized approach base on conjugated gradient technique (CGM)[25] and the second one is a non-linear hybrid method (HM).[6] Both methods have been well documented in the past, and we provide only a rapid description of their main features for consistency.

1. Conjugated gradient method: CGM

The basic idea underlying the CGM solution is to build up iteratively a sequence of the sought permittivity contrast χ within Ω by minimizing a cost functional of the form

$$\mathcal{F}_n(\chi_n) = \frac{\|\mathbf{h}_{l,n}\|_\Gamma^2}{\sum_{l=1}^{N} \|\mathbf{f}_l^{\text{mes}}\|_\Gamma^2} = W_\Gamma \sum_{l=1}^{N} \|\mathbf{h}_{l,n}\|_\Gamma^2 \tag{6}$$

with $\mathbf{h}_{l,n} = \mathbf{f}_l^{\text{mes}} - \mathbf{B}\chi_n\mathbf{E}_{l,n}$ is the residual error computed from Eq. (5), which represents the discrepancy between the measured scattered field and the simulated scattered field of the estimation χ_n. The subscript Γ in the norm $\|.\|$ and later in the inner product $\langle ., . \rangle$ indicates that the integration is performed over the receivers. The total field $\mathbf{E}_{l,n}$ is the solution of the self consistent equation with the contrast distribution χ_{n-1} : $\mathbf{E}_{l,n} \approx \mathbf{E}_{l,n-1} = [\mathbf{I} - \mathbf{A}\chi_{n-1}]^{-1}\mathbf{E}_l^{\text{inc}}$. At each iteration step n, the permittivity contrast distribution χ_n is built up according to the following recursive relation:

$$\chi_n = \chi_{n-1} + \beta_n d_n, \tag{7}$$

where the updated contrast χ_n is deduced from the previous one, χ_{n-1}, by adding an updating term $\beta_n d_n$. This correction term is composed of two factors: a real valued scalar weight β_n and an updating direction d_n. The scalar weight β_n is determined by minimizing the cost functional $\mathcal{F}_n(\chi_n)$. Substituting the expression of the parameter of interest χ_n Eq. (7) into the cost functional Eq. (6) leads to a polynomial expression with respect to the scalar weight β_n

$$\begin{aligned}\mathcal{F}_n(\chi_n) = F(\beta_n) = W_\Gamma \times \sum_{l=1}^{N} (&\|\mathbf{h}_{l,n-1}\|_\Gamma^2 + \beta_n^2 \|\mathbf{B}d_n\mathbf{E}_{l,n}\|_\Gamma^2 \\ &+ 2\beta_n \text{Re}\langle \mathbf{h}_{l,n-1} | \mathbf{B}d_n\mathbf{E}_{l,n} \rangle_\Gamma).\end{aligned} \tag{8}$$

The unique minimum of $F_n(\beta_n)$ is reached when $\frac{\partial F_n(\chi_n)}{\partial \beta_n} = 0$

$$\beta_n = W_\Gamma \sum_{l=1}^{N} \frac{\text{Re}\langle \mathbf{h}_{l,n-1} | \mathbf{B}d_n\mathbf{E}_{l,n} \rangle_\Gamma}{\|\mathbf{B}d_n\mathbf{E}_{l,n}\|_\Gamma^2}. \tag{9}$$

As for the updating direction d_n, we take the standard Polak-Ribière conjugate-gradient directions. With CGM, the improvement condition is not satisfied, i.e., the minimized function does not always decrease,[6] in particular, in the presence of high level of noise or in the multiple scattering regime. In this case, the final reconstruction result is chosen to be the one corresponding to the lowest value of the minimized cost function.

The first estimate for χ^{init} is derived from the backpropagation procedure.[26,27] We define a polarization density as

$$\mathbf{P}_l^{\text{init}} = \chi^{\text{init}}\mathbf{E}_l^{\text{init}} = \gamma_l \mathbf{B}^\dagger \mathbf{f}_l^{\text{mes}}, \tag{10}$$

where $\mathbf{B}^\dagger$ denotes the transpose complex conjugate matrix of the matrix $\mathbf{B}$. The scalar weight γ_l is determined by minimizing the cost function $H(\gamma_l)$ describing the discrepancy between the data $\mathbf{f}_l^{\text{mes}}$ and those that would be obtained with $\mathbf{P}_l^{\text{init}}$

$$H(\gamma_l) = \|\mathbf{f}_l^{\text{mes}} - \mathbf{B}\mathbf{P}_l^{\text{init}}\|_\Gamma = \|\mathbf{f}_l^{\text{mes}} - \gamma_l \mathbf{B}\mathbf{B}^\dagger \mathbf{f}_l^{\text{mes}}\|_\Gamma. \tag{11}$$

Writing down the necessary condition $\partial H/\partial \gamma_l = 0$ for H to be minimum leads to an analytic expression of γ_l

$$\gamma_l = \frac{\langle \mathbf{B}\mathbf{B}^\dagger \mathbf{f}_l^{\text{mes}} | \mathbf{f}_l^{\text{mes}} \rangle_\Gamma}{\|\mathbf{B}\mathbf{B}^\dagger \mathbf{f}_l^{\text{mes}}\|_\Gamma}. \tag{12}$$

Once the estimation of $\mathbf{P}^{\text{init}}$ is determined, an estimation of the total field $\mathbf{E}_l^{\text{init}}$ in the investigating domain can be derived as $\mathbf{E}_l^{\text{init}} = \mathbf{E}_l^{\text{inc}} + \mathbf{A}\mathbf{P}_l^{\text{init}}$. Finally, the initial guess for the permittivity distribution χ^{init} is given by the backpropagation method

$$\varepsilon^{\text{init}}(\mathbf{r}) = 1 + \text{Re}\left\{ \frac{\sum_{l=1}^{L} \mathbf{P}_l^{\text{init}}(\mathbf{r}).\bar{\mathbf{E}}_l^{\text{init}}(\mathbf{r})}{\sum_{l=1}^{L} \|\mathbf{E}_l^{\text{init}}(\mathbf{r})\|^2} \right\}, \tag{13}$$

where $\bar{x}$ is the complex conjugate of x.

2. DORT with conjugated gradient method: DORT-CGM

It has been shown that the backpropagation of the emergent singular vectors provides a means for generating new

incident fields focusing onto a given scatterer.[5] We propose here to introduce this information in the inversion procedure.

In the DORT-CGM inversion procedure, the focusing field derived from Eq. (2) is considered as the new incident field for the inverse scattering problem. We consider only the DORT singular vectors that are associated with the most significant singular values. Then, instead of the original fields $\mathbf{E}_{l,\alpha}^{\text{inc}}$ and $\mathbf{f}_l^{\text{mes}}$, we consider N_{DORT} incident backpropagated DORT fields $\mathbf{E}_p^{\text{DORT}}$ and N_{DORT} associated scattered fields $\mathbf{f}_p^{\text{DORT}}$ in the iterative scheme. Henceforth, the contrast permittivity distribution within the investigating domain Ω is determined iteratively by minimizing a cost functional which reads at the iteration step n

$$\mathcal{F}_n^{\text{DORT}}(\chi_n) = \frac{\sum_{p=1}^{N_{\text{DORT}}} \|\mathbf{h}_{p,n}^{\text{DORT}}\|_\Gamma^2}{\sum_{p=1}^{N_{\text{DORT}}} \|\mathbf{f}_p^{\text{DORT}}\|_\Gamma^2}, \tag{14}$$

where the residual error $\mathbf{h}_{p,n}^{\text{DORT}}$ is defined as $\mathbf{h}_{l,n}$

$$\mathbf{h}_{p,n}^{\text{DORT}} = \mathbf{f}_p^{\text{DORT}} - \mathbf{B}\chi_n \mathbf{E}_{p,n}^{\text{DORT;tot}}. \tag{15}$$

The updating directions are taken to be of the same form as the ones described in Section III B 1, where the involved gradients are computed from the cost functional $\mathcal{F}_n^{\text{DORT}}$ instead of $\mathcal{F}_n$. The initial guess of the permittivity is computed through the footprint of the sum of the intensities of the backpropagated dominant DORT fields

$$\varepsilon^{\text{init}}(\mathbf{r}) = 1 + 0.1 \times \left\{ \frac{\sum_{p=1}^{N_{\text{DORT}}} \|\mathbf{E}_p^{\text{DORT}}(\mathbf{r})\|_\Omega^2}{\max_\Omega \left[\sum_{p=1}^{N_{\text{DORT}}} \|\mathbf{E}_p^{\text{DORT}}(\mathbf{r})\|_\Omega^2 \right]} \right\}. \tag{16}$$

In Eq. (16), the maximum permittivity contrast of the initial guess has been set to 0.1. This value, which corresponds to the maximum contrast that is generally obtained with the backpropagation procedure, Eqs. (10) and (11), ensures that the light scattered by the first estimate satisfies Born approximation and that it is of the same order of magnitude as the backpropagation procedure, Eq. (13).

3. Hybrid method (HM), with DORT (DORT-HM)

The hybrid method has already been detailed in previous publications,[5,28] and only its main features are recalled here. It retrieves simultaneously the sample permittivity contrast χ and the total field $\mathbf{E}_l$ in the investigation domain. At each iteration step n, the cost functional reads

$$\mathcal{F}_n(\chi_n, \mathbf{E}_{l,n}) = \frac{\sum_{l=1}^{L} \|\mathbf{h}_{l,n}\|_\Gamma^2}{\sum_{l=1}^{L} \|\mathbf{f}_l^{\text{mes}}\|_\Gamma^2} + \frac{\sum_{l=1}^{L} \|\mathbf{g}_{l,n}\|_\Omega^2}{\sum_{l=1}^{L} \|\mathbf{E}_l^{\text{inc}}\|_\Omega^2}, \tag{17}$$

where $\mathbf{g}_{l,n}$ is a residual error on the field inside the investigating domain

$$\mathbf{g}_{l,n} = \mathbf{E}_l^{\text{inc}} - \mathbf{E}_{l,n} + \mathbf{A}\chi_n \mathbf{E}_{l,n}. \tag{18}$$

The minimization is performed using the Hybrid Method (HM) described in Ref. 6. In order to take into account the focusing fields derived from the SVD, the original scattered and incident fields are changed to $\mathbf{f}_p^{\text{DORT}}$ and $\mathbf{E}_p^{\text{DORT}}$, respectively. The iteration process is stopped when the cost function reaches a plateau.

IV. RECONSTRUCTION OF DIFFERENT TARGETS FROM EXPERIMENTAL MICROWAVE DATA

In this section, we compare the reconstructions given by the inversion methods, with and without DORT preprocessing, of different targets taken from the microwave database presented in Ref. 29. These data are particularly suited for our comparisons because many inversion techniques have already been applied to these measurements.

A. Experimental configuration and targets geometry

The experimental configuration is depicted in Fig. 1, for more details on the set-up see Refs. 30 and 31. The incident wave is assumed to be a plane wave propagating in the (x, y) plane with θ_{inc} ranging from 0° to 350° with a step 10° (green line) and polarized along z direction ($\phi_{\text{inc}} = 90°$), which corresponds to $L = 36$ emitters.

The receiver positions are indicated by the polar angle θ_{diff} ranges from 0° to 320° with the angular step 40° and the azimuthal angle ϕ_{diff} ranges from 30° to 150° with the angular step 15° (red line) yielding 81 different observation directions. For each position, the receiving antennas are oriented along x, y, and z axes in order to record the full vectorial scattered field. Following our notations, the detection configuration corresponds to $Q = 3 \times 81$ receivers. The background medium is air, $\varepsilon_b = 1$.

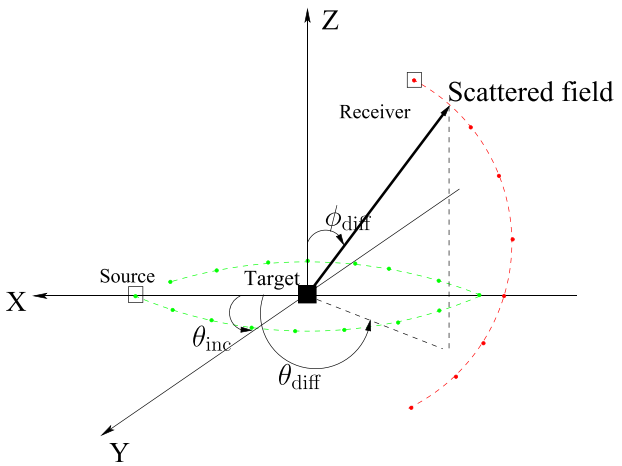

FIG. 1. Sketch of the experimental setup.[29] The illumination is performed in the (x, y) plane with θ_{inc} varying from 0° to 350° step 10° (green line). The observation angle θ_{diff} varies from 0° to 320° step 40° and ϕ_{diff} from 30° to 150° step 15° (red line).

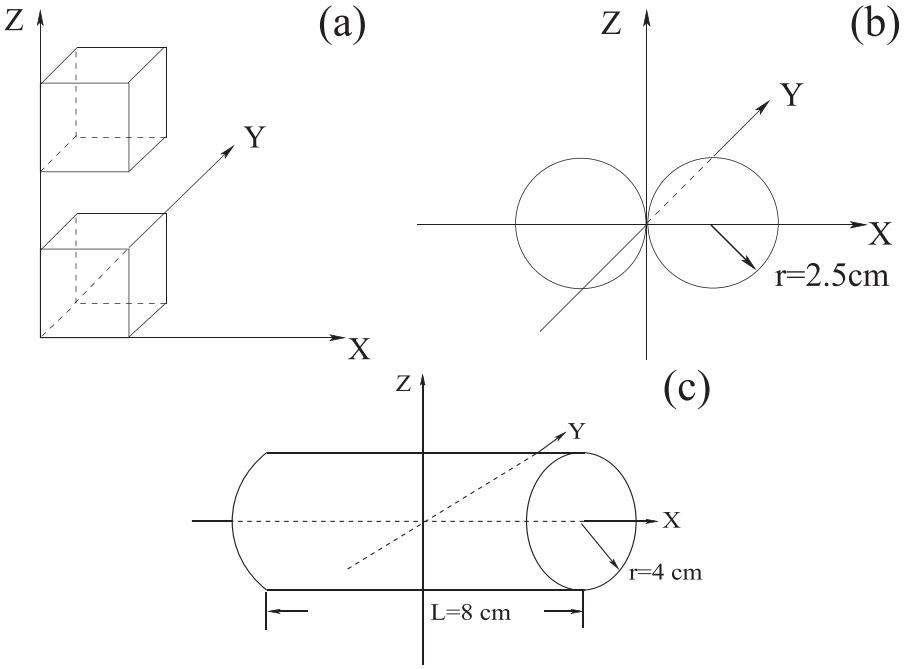

FIG. 2. Geometry of the targets. (a) Target A: Two dielectric cubes of relative permittivity $\varepsilon = 2.4$ and of side $a = 2.5$ cm located at ($a/2$, $a/2$, $a/2$) and ($a/2$, $a/2$, $5a/2$). (b) Target B: Two dielectric spheres in contact of relative permittivity $\varepsilon = 2.6$ and radius $r = 2.5$ cm located at ($-r$, 0, 0) and (r, 0, 0). (c) Target C: Cylinder of radius $r = 4$ cm, length $L = 8$ cm, with relative permittivity $\varepsilon = 3.05$.

Three different targets are considered in this work. The first one [Fig. 2(a)] is made of two cubes placed along the z-axis of relative permittivity $\varepsilon = 2.4$ and of side size $a = 2.5$ cm, and separated along the z-axis by 5 cm. It is illuminated at the operating frequency 8 GHz so that the side of each cube is about one wavelength inside the object ($\lambda/\sqrt{\varepsilon} \approx a$).

The second one is made of two dielectric spheres of relative permittivity $\varepsilon = 2.6$ and of radius $r = 2.5$ cm in contact, as shown in Fig. 2(b). The operating frequency is 4 GHz so that the diameter of each sphere corresponds again to one wavelength inside the object ($\lambda/\sqrt{\varepsilon} \approx 2r$). Target B is more difficult to reconstruct than target A because the two spheres are in contact.

Last, target C is a cylinder of length 8 cm, radius 4 cm, and permittivity 3.05. In this case, the operating frequency is 3 GHz. This target is more difficult to reconstruct than targets A and B because its size is almost 1.5 times the wavelength in the object and its permittivity is high. To our knowledge, all the inversion methods without regularization that have tackled this problem (including the CGM and HM) failed.[25,29,32,33] Thus, target C is a particularly good example for pointing out the interest of DORT preprocessing.

In a classical DORT procedure, the key point is to determine the number of useful singular values, N_{DORT}, which will be retained in the inversion. In Fig. 3, we plot the singular values of the scattering matrix for each target. All curves exhibit a discontinuity when the singular value reaches $\sigma = 0.07$. The experiments being performed with the same additive noise, the latter can be interpreted as a boundary between the signal and noise space. From these evolution curves, one infers that the number of dominant singular values for target A is five while it is nine for target B and sixteen for target C. As expected, the number of dominant singular values increases with the target size.

Note however that, in our approach, the DORT illuminations are weighted by their corresponding singular values, Eq. (2). When the singular values are weak, the associated scattered fields (Eq. (3)) contribute marginally to the cost functional. Thus, with our formulation, the removal of the noise space is not really necessary. It is essentially useful to decrease the number of data and the computation time.

B. Reconstructions

For all the inversions, the investigation domain is a bounded box Ω sized $(12.5 \times 12.5 \times 12.5)$ cm^3 and its discretization size is taken equal to $d = 0.5$ cm, which is smaller than one sixth of the wavelength whatever the experiment. In all the reported results, only the real part of the reconstructed permittivity is displayed, the imaginary part being always very small.

In this section, we compare the final reconstructions given by the classical conjugated gradient method (CGM), the classical hybrid inversion method (HM), the conjugated gradient method combined with DORT procedure (DORT-CGM), and the hybrid method combined with the DORT procedure (DORT-HM), for target A, Fig. 4; target B, Fig. 5;

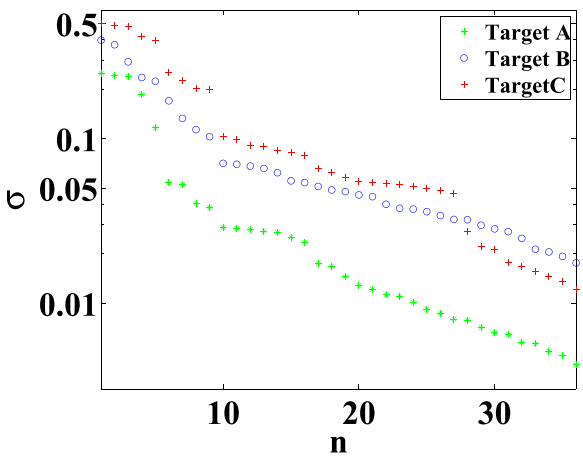

FIG. 3. Evolution curves of the singular values for target A (*), target B (○), and target C (+).

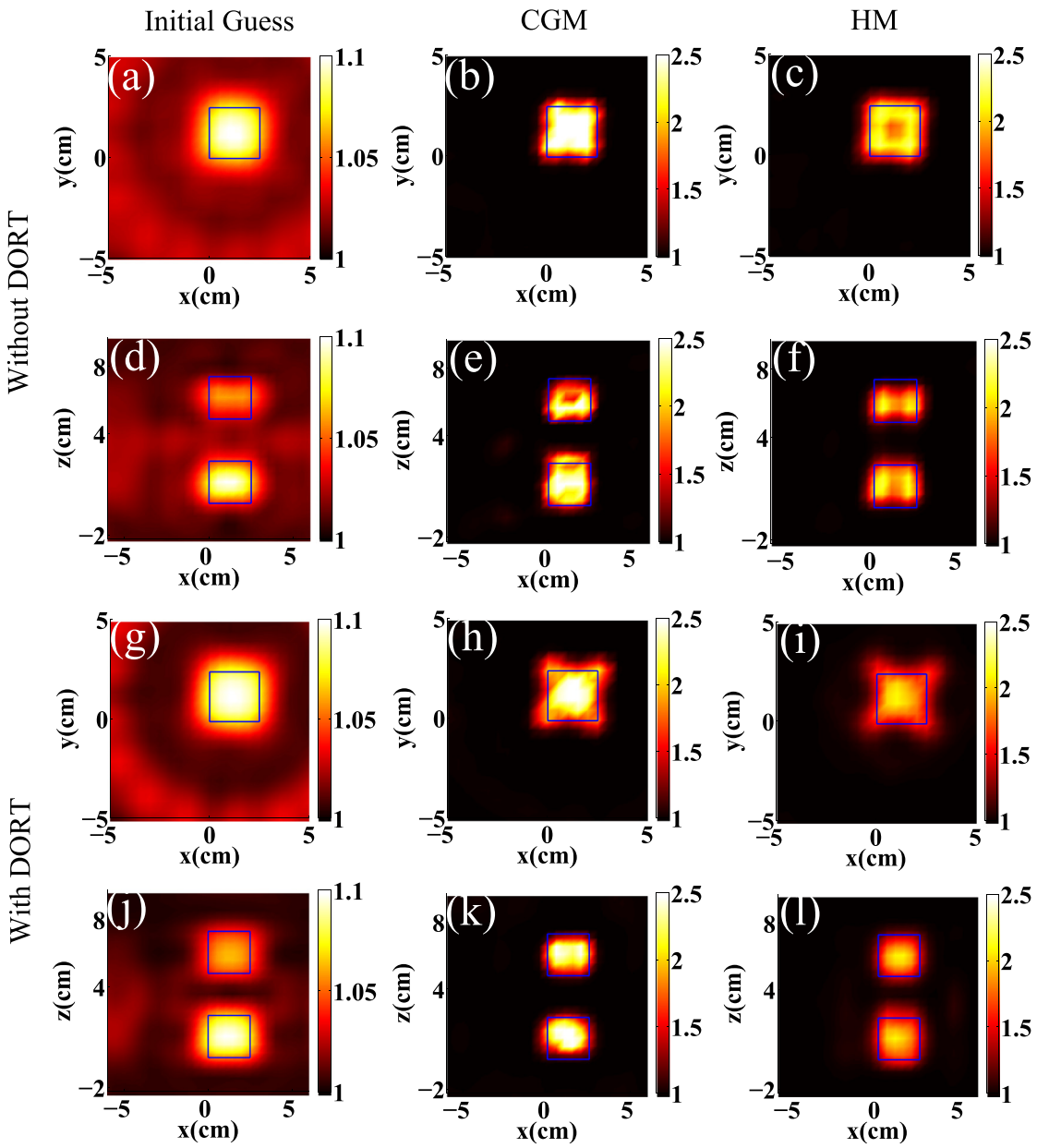

FIG. 4. Cut of the reconstructed permittivity of target A (two cubes along the z-axis) displayed in Fig. 2(a) using different inversion schemes. (a)–(c) and (g)–(i): in the (x, y) plane at $z = 1.25$ cm. (d)–(f) and (g)–(l): in the (x, z) plane at $y = 1.25$ cm. (a) and (d) permittivity obtained by the classical backpropagation procedure, see Eq. (13). (g) and (j) Permittivity obtained with DORT, see Eq. (16). (b) and (e) Reconstruction using CGM. (c) and (f) Reconstruction using HM. (h) and (k) Reconstruction using DORT-CGM. (i) and (l) Reconstruction using DORT-HM.

and target C, Fig. 6. In addition, we display the initial estimates of the methods, either given by the backpropagation technique Eq. (13)[26,27] and/or by the DORT intensity map, Eq. (16).

To quantify the quality of the images, a contrast reconstruction error is defined as

$$\mathrm{Err}_\chi = \frac{\|\chi_{\mathrm{actual}} - \chi_{\mathrm{rec}}\|_\Omega^2}{\|\chi_{\mathrm{actual}}\|_\Omega^2}. \tag{19}$$

From Figs. 4–6 and Table I, it is first seen that HM is always superior to CGM for inverting the experimental data. This observation is in agreement with previous studies by analyzing the performances of the linearized and non-linear inversion schemes.[34]

Second, whatever the inversion technique, the DORT preprocessing ameliorates the target reconstruction. It reduces the permittivity inhomogeneities inside the objects, renders the value of the estimated permittivity closer to the actual one, and in the case of target C, it is mandatory for getting an accurate permittivity distribution. It is worth recalling that, because of its size and high permittivity contrast, target C is very difficult to retrieve.[25,33,35,36] Sole regularized inversion techniques were able to reconstruct it relatively accurately.[7,8] Here, using the DORT preprocessing and without any regularization, we are able to reconstruct the cylinder with DORT-HM. Our approach yields an estimation of the relative permittivity of about 3 (for an actual value of 3.05), while the regularized techniques obtained an estimation of the relative permittivity about 2.[7,8]

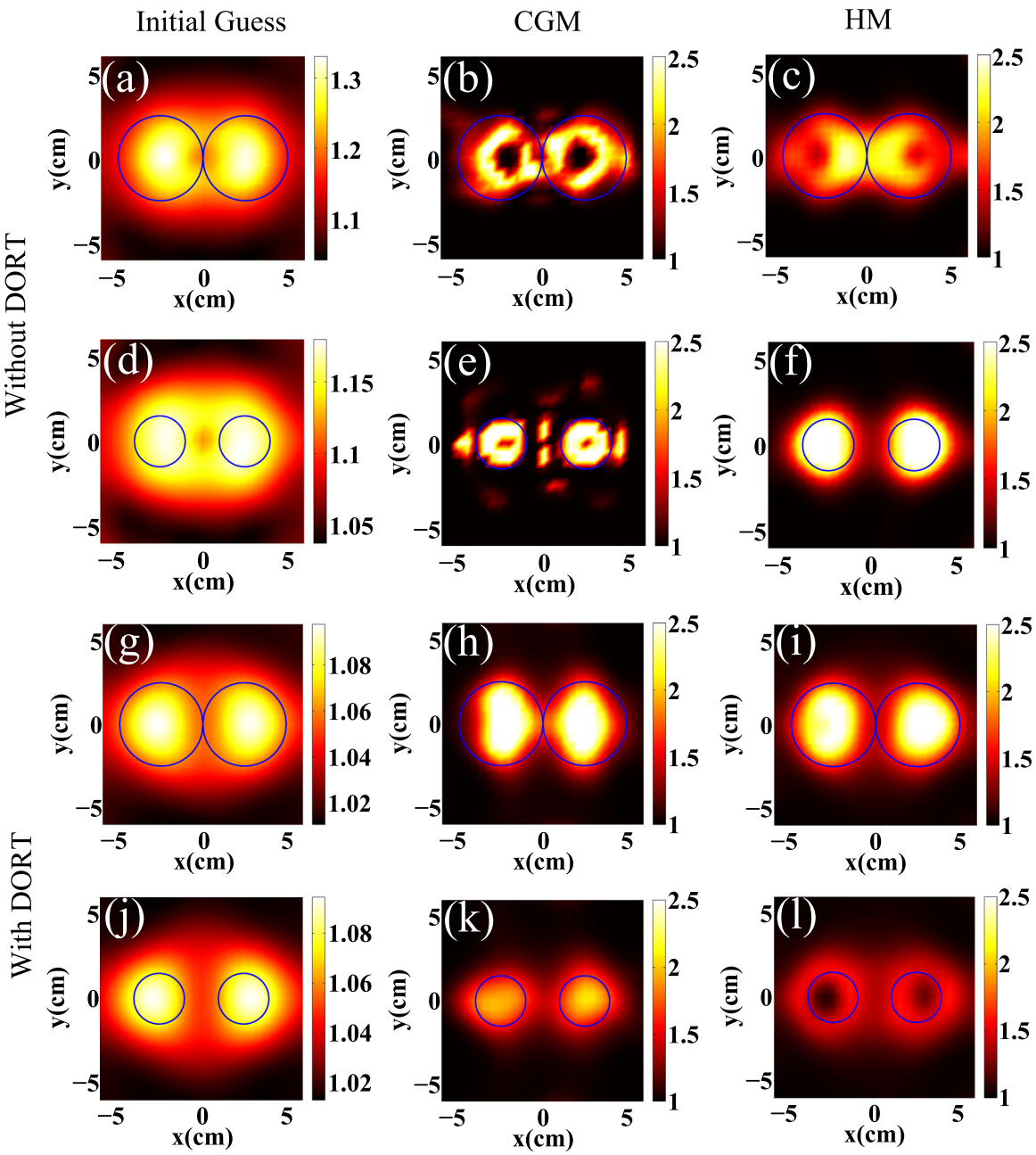

FIG. 5. Cut of the reconstructed permittivity of the target B (two spheres in contact), displayed in Fig. 2(b) using different inversion schemes. (a)–(c) and (g)–(i): in the (x, y) plane at $z = 0$ cm. (d)–(f) and (g)–(l): in the (x, y) plane at $z = -1.25$ cm. (a) and (d) Permittivity obtained by the classical backpropagation procedure. (g) and (j) Permittivity obtained with DORT. (b) and (e) Reconstruction using CGM. (c) and (f) Reconstruction using HM. (h) and (k) Reconstruction using DORT-CGM. (i) and (l) Reconstruction result using DORT-HM.

One interest of the DORT procedure is that it provides an initial estimate that is significantly better than that given by the backpropagation technique. Although some high order singular vectors have been known to backpropagate outside the support of the object, the weighting of the backpropagated DORT fields with their associated singular values ensures the dominance of the singular vectors that are the least sensitive to noise. Now the latter are usually producing field maps that are confined in the target volume. When the objects are small compared to the wavelength, backpropagation and DORT intensity maps are basically equivalent as shown in Ref. 37 and observed in Fig. 4. On the other hand, when the target size is comparable to or larger than the wavelength as in case C, the DORT guess is clearly better than the backpropagation guess and even retrieves the shape of the target. These results suggest that the DORT intensity map could even be used alone, as a cheap direct inversion scheme.

In addition, introducing the DORT procedure in the inversion algorithm decreases the influence of the noisy data via the weighting of the cost functional, and it limits the search directions of the optimization process to the target support via the use of focusing illuminations.

Another advantage of the DORT procedure is that it permits a significant decrease of the computation time, as can

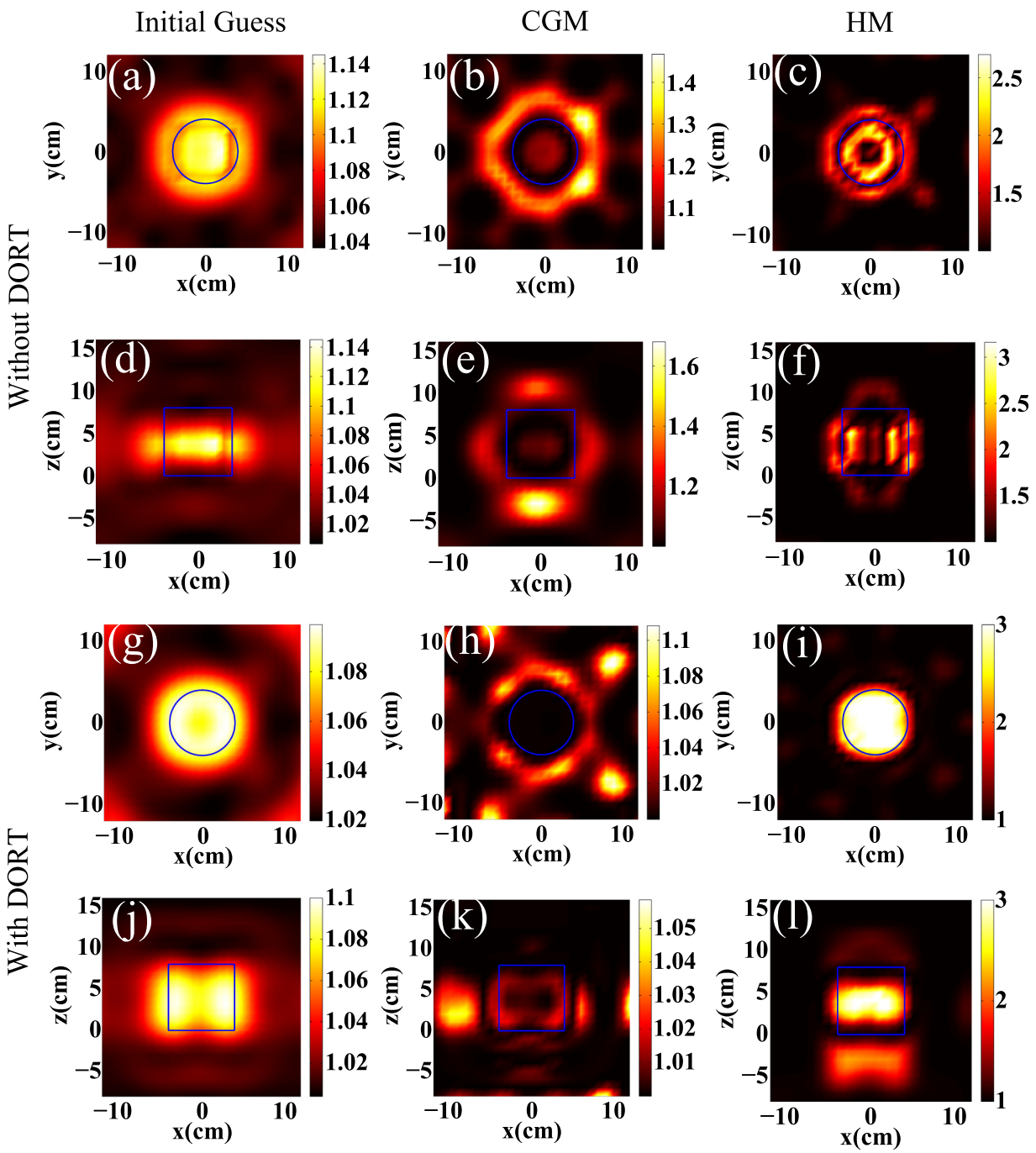

FIG. 6. Cut of the reconstructed permittivity of the target C displayed in Fig. 2(c) using different inversion schemes. (a)–(c) and (g)–(i): in the (x, y) plane at $z = 0$ cm. (d)–(f) and (g)–(l): in the (x, z) plane at $y = 0$ cm. (a) and (d) Permittivity map obtained by the classical backpropagation procedure. (g) and (j) Permittivity map obtained with DORT. (b) and (e) Reconstruction using CGM. (c) and (f) Reconstruction using HM. (h) and (k) Reconstruction using DORT-CGM. (i) and (l) Reconstruction using DORT-HM.

be seen in Table II. This comes from the fact that the computational burden is directly proportional to the number of illuminations and that the DORT illuminations with the weakest singular values have been discarded in the inversion process. It is worth recalling at this point that because of the weighting of the DORT illuminations with their associated singular values, discarding the weakest illuminations has quasi no impact on the reconstructions. By contrast, keeping the dominant illuminations without any weighting yields significantly deteriorated reconstructions (not shown). Thus, the truncation of the singular vector matrix is interesting for accelerating the inversion, but the weighting is mandatory for improving the reconstructions.

Lastly, we have conducted a rapid study on the noise sensibility of the DORT inversion schemes by adding numerical white noise with increasing magnitude to the experimental data of Target A. It was observed that the first singular value increased with noise, reinforcing the dominance of the first DORT vector over the others in the weighted inversion procedure. The first singular vector conveying essentially information on the target low frequencies, the resolution was deteriorated but the reconstruction remained stable.

TABLE I. Contrast error Err_χ in % for the different targets and for the different inversion methods.

	DORT-CGM	CGM	DORT-HM	HM
Target A	58%	84%	53%	78%
Target B	40%	268%	37%	34%
Target C	483%	207%	74%	109%

TABLE II. Computation time and the number of iteration for CGM, DORT-CGM, HM, and DORT-HM. The star indicates that the inversion scheme did not converge: the iteration number has been chosen to yield the smallest value of cost functional. (The better stabilized DORT-CGM achieves lower cost functionals than CGM with slightly more iterations.)

		DORT-CGM	CGM	DORT-HM	HM
Target A	Iteration number	23*	20*	15	10
	Computation time (s)	520	1570	421	1426
Target B	Iteration number	41*	30*	10	10
	Computation time (s)	700	9900	460	1426
Target C	Iteration number	10*	2*	10	10
	Computation time(s)	340	278	871	2083

V. CONCLUSION

In an imaging experiment, the illuminations are not necessarily adapted to the target under observation. From the Singular Value Decomposition of the scattering matrix, it is possible to synthesize incident fields, named DORT fields, that focus preferentially on the target. We show that replacing the initial illuminations by the DORT fields in the inversion schemes yields a significant amelioration of the reconstructions together with a decrease in the computation time. The interest of DORT preprocessing is particularly evident when the target size is comparable or larger than the imaging wavelength and when non-linearized inversion schemes are used. Hence, in addition to the well known interest of DORT illuminations for focusing on small targets in a cluttered environment, DORT preprocessing is also most useful for imaging large targets using non-linearized inversion tools.

ACKNOWLEDGMENTS

This work has been financed by the ANR SURMITO, Grant No. 12BS03 006 01.

[1]A. Sentenac, C.-A. Guérin, P. C. Chaumet, F. Drsek, H. Giovannini, N. Bertaux, and M. Holschneider, "Influence of multiple scattering on the resolution of an imaging system: A Cramer-Rao analysis," Opt. Express **15**, 1340 (2007).
[2]D. Colton, *Inverse Acoustic and Electromagnetic Scattering Theory*, Applied Mathematical Sciences, 2nd ed. (Springer-Verlag, 1998).
[3]Z. Q. Zhang and Q. H. Liu, "Three-dimensional nonlinear image reconstruction for microwave biomedical imaging," IEEE Trans. Biomed. Eng. **51**, 544 (2004).
[4]W. Hu, A. Abubakar, and T. M. Habashy, "Simultaneous multifrequency inversion of full-waveform seismic data," Geophysics **74**, R1 (2009).
[5]T. Zhang, P. C. Chaumet, E. Mudry, A. Sentenac, and K. Belkebir, "Electromagnetic wave imaging of targets buried in a cluttered medium using a hybrid inversion-dort method," Inverse Prob. **28**, 125008 (2012).
[6]E. Mudry, P. C. Chaumet, K. Belkebir, and A. Sentenac, "Electromagnetic wave imaging of three-dimensional targets using a hybrid iterative inversion method," Inverse Prob. **28**, 065007 (2012).
[7]C. Yu, M. Yuan, and Q. H. Liu, "Reconstruction of 3d objects from multi-frequency experimental data with a fast dbim-bcgs method," Inverse Prob. **25**, 024007 (2009).
[8]M. Li, A. Abubakar, and P. M. van den Berg, "Application of the multiplicative regularized contrast source inversion method on 3d experimental fresnel data," Inverse Prob. **25**, 024006 (2009).
[9]C. Prada, S. Manneville, D. Spoliansky, M. Finkand, and M. Fink, "Decomposition of the time reversal operator: Detection and selective focusing on two scatterers," J. Acoust. Soc. Am. **99**, 2067–2076 (1996).
[10]D. Q. Nguyen and W. S. Gan, "The DORT solution in acoustic inverse scattering problem of a small elastic scatterer," Ultrasonics **50**, 829–840 (2010).
[11]C. Prada and M. Fink, "Eigenmodes of the time reversal operator: a solution to selective focusing in multiple-target media," Wave Motion **20**, 151–163 (1994).
[12]C. D. Moss, F. L. Teixeira, and J. A. Kong, "Detection of targets in continuous random media: A numerical study using the angular correlation function," Microwave Opt. Technol. Lett. **33**, 242–247 (2002).
[13]T. Zhang, C. Godavarthi, P. C. Chaumet, G. Maire, H. G. nnini, A. Talneau, C. Prada, A. Sentenac, and K. Belkebir, "Tomographic diffractive microscopy with agile illuminations for imaging targets in a noisy background," Opt. Lett. **40**, 573–576 (2015).
[14]A. Dubois, K. Belkebir, and M. Saillard, "Localization and characterization of two-dimensional targets buried in a cluttered environment," Inverse Prob. **20**, S63–S79 (2004).
[15]M. E. Yavuz and F. L. Teixeira, "Full time-domain DORT for ultrawideband electromagnetic fields in dispersive, random inhomogeneous media," IEEE Trans. Antennas Propag. **54**, 2305–2315 (2006).
[16]L. Borcea, G. Papanicolaou, C. Tsogka, and J. Berryman, "Imaging and time reversal in random media," Inverse Prob. **18**, 1247 (2002).
[17]D. H. Chambers and J. G. Berryman, "Target characterization using decomposition of the time-reversal operator: electromagnetic scattering from small ellipsoids," Inverse Prob. **22**, 2145 (2006).
[18]L. Chehami, E. Moulin, J. de Rosny, C. Prada, O. B. Matar, F. Benmeddour, and J. Assaad, "Detection and localization of a defect in a reverberant plate using acoustic field correlation," J. Appl. Phys. **115**, 104901 (2014).
[19]L. Borcea, G. Papanicolaou, and C. Tsogka, "Theory and applications of time reversal and interferrometric imaging," Inverse Prob. **19**, S139–S164 (2003).
[20]P. C. Hansen, "The truncated SVD as a method for regularization," BIT Numer. Math. **27**, 534–553 (1987).
[21]P. C. Hansen, "Truncated singular value decomposition solutions to discrete ill-posed problems with ill-determined numerical rank," SIAM J. Sci. Stat. Comput. **11**, 503–518 (1990).
[22]X. Y. Zhang, H. Tortel, A. Litman, and J. M. Geffrin, "An extended-DORT method and its application in a cavity configuration," Inverse Prob. **28**, 115008 (2012).
[23]E. M. Purcell and C. R. Pennypacker, "Scattering and absorption of light by nonspherical dielectric grains," Astrophys. J. **186**, 705–714 (1973).
[24]B. T. Draine, "The discrete-dipole approximation and its application to interstellar graphite grains," Astrophys. J. **333**, 848–872 (1988).
[25]P. C. Chaumet and K. Belkebir, "Three-dimensional reconstruction from real data using a conjugate gradient-coupled dipole method," Inverse Prob. **25**, 024003 (2009).
[26]K. Belkebir, S. Bonnard, F. Pezin, P. Sabouroux, and M. Saillard, "Validation of 2D inverse scattering algorithms from multi-frequency experimental data," J. Electromagn. Waves Appl. **14**, 1637–1667 (2000).
[27]K. Belkebir, P. C. Chaumet, and A. Sentenac, "Superresolution in total internal reflection tomography," J. Opt. Soc. Am. A **22**, 1889–1897 (2005).
[28]G. Maire, Y. Ruan, T. Zhang, P. C. Chaumet, H. Giovannini, D. Sentenac, A. Talneau, K. Belkebir, and A. Sentenac, "High-resolution tomographic diffractive microscopy in reflection configuration," J. Opt. Soc. Am. A **30**, 2133–2139 (2013).
[29]J. M. Geffrin and P. Sabouroux, "Continuing with the Fresnel database: Experimental setup and improvements in 3D scattering measurements," Inverse Prob. **25**, 024001 (2009).
[30]C. Eyraud, J.-M. Geffrin, P. Sabouroux, P. C. Chaumet, H. Tortel, H. Giovannini, and A. Litman, "Validation of 3D bistatic microwave scattering measurement setup," Radio Sci. **43**, RS4018, doi:10.1029/2008RS003836 (2008).

[31]J.-M. Geffrin, P. C. Chaumet, C. Eyraud, K. Belkebir, and P. Sabouroux, "Electromagnetic three-dimensional reconstruction of targets from free space experimental data," Appl. Phys. Lett. **92**, 194103 (2008).
[32]I. Catapano, K. Belkebir, and J.-M. Geffrin, "A single-view imaging strategy for transient scattered fields," Inverse Prob. **24**, 015008 (2008).
[33]J. D. Zaeytijd and A. Franchois, "Three-dimensional quantitative microwave imaging from measured data with multiplicative smoothing and value picking regularization," Inverse Prob. **25**, 024004 (2009).
[34]K. Belkebir and M. Saillard, "Special section: Testing inversion algorithms against experimental data," Inverse Prob. **17**, 1565–1571 (2001).
[35]I. Catapano, L. Crocco, M. D. Urso, and T. Isernia, "3d microwave imaging via preliminary support reconstruction: Testing on the fresnel 2008 database," Inverse Prob. **25**, 024002 (2009).
[36]C. Eyraud, A. Litman, A. Hérique, and W. Kofman, "Microwave imaging from experimental data within a bayesian framework with realistic random noise," Inverse Prob. **25**, 024005 (2009).
[37]G. Micolau, "Etude théorique et numérique de la méthode de la Décomposition de l'Opérateur de Retournement Temporel (D.O.R.T) en diffusion électromagnétique," Ph.D. thesis (Université Aix Marseille, France, 2001).